RSC Advances

PAPER

View Article Online
View Journal | View Issue

Cite this: *RSC Adv.*, 2024, **14**, 11584

An efficient β-nucleating agent with high lattice matching rate for plate-like crystallization of polypropylene random copolymer

Bo Wu, [ab] Xian Zheng,[b] Yanwei Ren, [a] Hailong Yu,[b] Haiqiang Leng,[b] Yubo Wang[a] and Huanfeng Jiang *[a]

It is challenging to naturally produce large amounts of β-crystals by directly adding a commercial β-nucleating agent (β-NA) into polypropylene random copolymer (PPR) at present. In this work, a novel rare earth β-NA WBN-28 was directly introduced into PPR to prepare β-PPR with high β-crystal conversion. The results of differential scanning calorimetry (DSC) and wide-angle X-ray diffraction (WAXD) indicated that it is an efficient β-NA for PPR. The β-conversion rate (β-CR) could surpass 85% when the nucleating agent content was mere 0.05%. With the further increment of nucleating agent, the β-CR increased gradually, which could reach 89.5% and 86.9% respectively calculated by DSC and WAXD when the addition amount was 0.4%. The incredible high β-CR delayed the βα-recrystallization in isothermal crystallization. The fusion peak of α-crystal was unobserved below the isothermal crystallization temperature of 122 °C when the addition amount was more than 0.2%. Furthermore, there was a highly ordered structure in WBN-28 with the periodicity of 12.89 Å, which was approximately twice of the unit cell parameter in the *c* direction of β-PP, indicating a high lattice matching rate between them. Intuitively observed by polarizing optical microscope (POM), the crystal grains of the blends with β-NA were more refined and finally crystallized in a plate-like shape. The forming process of the plate-like β crystalline regions were proposed by scanning electron microscope (SEM) and POM.

Received 12th December 2023
Accepted 3rd April 2024

DOI: 10.1039/d3ra08484a

rsc.li/rsc-advances

1 Introduction

Polypropylene traditionally includes homopolymers (PPHs), block copolymers (PPBs) and random copolymers (PPRs).[1,2] As a general plastic, polypropylene possesses an extremely broad application in all walks of life.[3,4] The extrusion grade PPR has been widely used in the pipe industry because of its excellent characteristics such as acid and alkali corrosion resistance, sound insulation, weldability and non-toxic.[5,6] To more significantly improve the brittleness of PPR at sub-zero, poor pressure resistance at elevated temperature and large thermal expansion coefficient, polypropene random crystallinity temperature (PP-RCT) has been born.[7] Compared with PPR, PP-RCT has marked advantages in temperature tolerance, pressure resistance and service life and additionally includes noticeable improvement in sub-zero toughness.[8] The long-term strength of PP-RCT is surpassing 50% higher than that of PPR after 50 years at 70 °C.[9] Therefore, the pipe wall of PP-RCT is thinner, and high extrusion speed can be properly used to reduce the amount of material and improve remarkably the production efficiency. Larger inner diameter pipe can be manufactured to increase sufficiently the volume capacity, which provides a solution to the typical problem of low-pressure water supply.[10]

β-NA is undoubtedly a key factor in the preparation of PP-RCT. At present, there are many typical kinds of β nucleating agents for polypropylene, including inorganic salts,[11,12] amides,[13–15] carboxylates,[16–18] rare earths[19,20] and even polymers.[21–23] Among them, amides,[24,25] carboxylates[26] and rare earths[27] are chiefly used for industrial applications. However, not all β-nucleating agents have excellent β-induced nucleation effect for PPR.[28] The nucleation effect of β-NA is often inhibited because of the presence of copolymerized ethylene units and the coexistence of polymorphs in PPR. The ethylene copolymerization units reduce the stereoregularity of the chain segment, therefore affecting the β-crystallization effect of PPR.[29,30] Additionally, if the β-NA is not effective enough to overcome the molecular chain defects of PPR, it will be vulnerable in the competition with α- and γ-crystals and ultimately affect the β-crystallization.[31,32] The same nucleating agent cannot gain the equivalent results as PPH in PPR, and the β-nucleating effect in PPR is ordinarily exceedingly worse than that in PPH.[33,34] Therefore, it is very challenging to procure high β-crystal content by directly adding β-NA into PPR.

Many effective efforts have been developed to significantly improve the β-CR in PPR during last marked decade. Nucleating agent supported on nanoparticles is one of the effective

[a]*School of Chemistry and Chemical Engineering, South China University of Technology, 381 Wushan Road, Guangzhou, 510641, China. E-mail: jianghf@scut.edu.cn; Fax: +86-20-87112906; Tel: +86-20-87112906*

[b]*Guangdong Winner New Materials Technology Co., Ltd., Foshan, 528521, China*

methods.[35,36] Li *et al.*[37] used calcium pimelate supported on the surface of nano-$CaCO_3$ as β-NA for PPR following the β-CR of PPR was enhanced. Besides, since Menyhárd *et al.*[38] found that polypropylene homopolymer can improve the β-crystallization of PPR, many researchers have focused on this area. Luo *et al.*[39] added moderate amounts of isotactic polypropylene into PPR to enhance the β-nucleated crystallization. They found stereoregular molecular chains in PPH benefit the formation of primary β-nuclei at the early stage of crystallization and ultimately improve β-crystallization. Li *et al.*[40] and Jiang *et al.*[41] utilized similar methods to introduce an appropriate amount of PPH into PPR, which significantly improved the β-crystallization effect of PPR and the toughness of the material. In recent studies, we have found an efficient β-NA WBN-28 for PPR. In this paper, the influence of WBN-28 on the melting and crystallization of PPR and the isothermal crystallization process have been analyzed. The morphological evolutions of PPR in isothermal crystallization were intuitively observed by POM. The probable nucleation mechanism has been explored *via* WAXD, POM and SEM. Without other auxiliary means, a very high β-CR can be gained by directly adding this β-NA into PPR and even a low addition of 0.05% produces an excellent effect. This work is beneficial to further understand the effect of β-NA on PPR β-modification and also undoubtedly provide a more appropriate choice for its engineering application.

2 Experimental section

2.1 Materials

Propylene–ethylene random copolymer used in this work was purchased from PetroChina Daqing Petrochemical with a commercial grade name of PA14D. It has a melt flow rate of 0.41 g/10 min (230 °C, 2.16 kg) and a weight-average molecular weight M_w of 4.78×10^5 g mol^{-1}. The ethylene content of PA14D was about 4.1%. The β-NA was a new kind of rare earth (trade name WBN-28, dimetal complexes of lanthanum and barium containing some specific ligands) kindly supplied by Guangdong Winner New Materials Co., Ltd. (Foshan, China).

2.2 Samples preparation

The PPR/β-NA samples with different nucleating agent content were prepared by using a corotating twin-screw extruder (TSJ-35, L/D ration = 40, manufactured by Nanjing Norda Machinergy Equipment Co., Ltd.). The processing temperature was set 165–205 °C from hopper to die and the screw speed was fixed at 300 rpm. The extruded strands were immediately quenched in water and then cut into pellets by a pelletizer. For more convenience, the samples are abbreviated as PPR/*x*NA, where the PPR resin is always 100%wt and *x* indicate the concentration of β-nucleating agent from 0.05% to 0.4%. For example, PPR/0.05NA means a compound with 100%wt PPR and 0.05%wt β-NA.

2.3 Differential scanning calorimetry (DSC)

The non-isothermal crystallization behavior of the specimens was recorded using a PerkinElmer Jade DSC using nitrogen as the purging gas. The samples were in the range of 5–7 mg. The heating rate was 10 °C min^{-1} in the first heating scanning from 50 °C to 210 °C, then the samples were kept at 210 °C for 5 min to eliminate the thermal history. The cooling rate was 10 °C min^{-1} in the cooling scanning from 210 °C to 50 °C and the crystallization exothermic peak was recorded. Subsequent heating scanning rate was 10 °C min^{-1} from 50 °C to 210 °C and the melting endothermic peaks were recorded.

The percentage of β-crystal of a sample, φ_β can be calculated according to:

$$X_\alpha = \frac{\Delta H_\alpha}{\Delta H_\alpha^0} \times 100\% \quad (1)$$

$$X_\beta = \frac{\Delta H_\beta}{\Delta H_\beta^0} \times 100\% \quad (2)$$

$$\varphi_\beta = \frac{X_\beta}{X_\alpha + X_\beta} \times 100\% \quad (3)$$

where X_α and X_β are the crystallinities of the α-crystal and β-crystal, ΔH_α and ΔH_β are the calibrated specific fusion heat of either the α-crystal and β-crystal, ΔH_α^0 and ΔH_β^0 are the standard fusion heat of the α-crystal and β-crystal which are 177 J g^{-1} and 168.5 J g^{-1},[42] respectively. Because the DSC curves of many samples exhibit both α-crystal and β-crystal, the fusion heat is calculated according to a correction method proposed in the literature.[43] The height of the vertical line from the highest point of the melting peak of β-crystal to the baseline is h_1, and the height of the vertical line from the lowest point of the two melting peaks of α-crystal and β-crystal to the baseline is h_2. At the same time h_2 divides the fusion heat into a β component ΔH_β^* and an α component. Since the less perfect α-crystals are melted before the α maximum point during heating and contribute to ΔH_β^*, the fusion heat of the β-crystal ΔH_β is approximated by a correcting equation:

$$A = \left(1 - \frac{h_2}{h_1}\right)^{0.6} \quad (4)$$

$$\Delta H_\beta = A \times \Delta H_\beta^* \quad (5)$$

$$\Delta H_\alpha = \Delta H - \Delta H_\beta \quad (6)$$

ΔH is the total fusion heat calculated from the DSC melting curve.

The isothermal crystallization behavior of the specimens was also recorded. The samples were heated to 210 °C for 5 min and then quenched to the desired crystallization temperature maintained constant until the crystallization was complete. After that, subsequent heating scanning rate was 10 °C min^{-1} from the desired crystallization temperature to 210 °C and the melting peaks were recorded.

2.4 Wide-angle X-ray diffraction (WAXD)

The samples were first held at 210 °C for 5 min and then cooled to 120 °C (according to the satisfactory results of isothermal crystallization experiment, 120 °C was chosen to be the isothermal crystallization temperature for XRD, SEM and POM samples.) for 2 hours. In the above process, the samples were

pressed into thin sheets about 0.2 mm. After that, the sheets were cooled to room temperature. The 2D-WAXD experiments were carried out with a D8 ADVANCE (BRUKER) diffractometer using Cu Kα radiation scanned from 5° to 60° at a speed of 6°/min. The wavelength of the X-ray was 0.154 nm at 40 kV and 40 mA. The data were processed by XRD pattern processing & identification (JADE 6.5). The relative amount of β-crystal was calculated according to Tuner-Jones equation:[44]

$$K_\beta = \frac{H_\beta(300)}{H_\beta(300) + H_{\alpha1}(110) + H_{\alpha2}(040) + H_{\alpha3}(130)} \times 100\% \quad (7)$$

in which, $H_\beta(300)$ is the intensity of (300) reflection of β-crystal and $H_{\alpha1}(110)$, $H_{\alpha2}(040)$ and $H_{\alpha3}(130)$ are the intensities of the (110), (040), (130) reflections of α-crystal, respectively.

2.5 Polarizing optical microscopy (POM)

The isothermal crystallization morphologies of the samples were observed *via* a Leica DM2700M polarizing optical microscope with a heating stage. The samples were heated to 220 °C for 5 min and pressed into thin sheets used by a cover-slip. After that, the samples were cooled to 120 °C at a rate of 50 °C min^{-1} on a heating stage.

2.6 Scanning electron microscopy (SEM)

All samples were firstly isothermally crystallized at 120 °C for 2 hours. Subsequently, the splines were cryogenically fractured in liquid nitrogen and the cryo-fractured surface immerged in a potassium permanganate solution[45] to etch the amorphous part of PPR in order to clearly observe the crystal structure. All samples were sputter-coated with gold powder for 240 S before test. Scanning electron microscopy (SEM) experiments were carried out with a SU8220 (HITACHI) instrument.

3 Results and discussion

3.1 DSC and WAXD analysis of PPR/NA

Fig. 1 shows the first cooling crystallization curves (a) and the following heating curves (b) of pure PPR and PPR with different contents of β-NA. From the graph (a), it can be observed that the crystallization peak of PPR visibly moves to elevated temperature direction, obviously improved even if in PPR/0.05NA. With a further increment of β-NA, the crystallization temperature increases slowly, reaching 105.1 °C in PPR/0.4NA. It can be observed from the graph (b) that conversion rate of β-crystal can reach 86.4% even if in PPR/0.05NA. From the melting curves, it can be identified that the fusion peaks of α-crystal and β-crystal are clearly separated, and there are fewer coexisting thawing regions. With the increment of the amount of nucleating agent, the conversion rate of β-crystal increases gradually, up to 89.5% in PPR/0.4NA. In addition, the fusion peaks of α-crystal and β-crystal can be obviously separated in each adding amount, indicating that WBN-28 is undoubtedly an efficient β-NA for PPR. The detailed data are summarized in Table 1. The corresponding enthalpy is naturally calculated by the secondary heating curves. In addition to the extremely satisfactory effect of typically inducing β-crystal, the appropriate addition of nucleating agent also gradually increases the total crystallinity of the system. It can reach 35.6% in PPR/0.4NA, which efficiently is 1.2 times that in pure PPR.

The isothermal crystallization of PPR/NA blends is further determined on the WAXD instrument. Fig. 2 is the WAXD test pattern of pure PPR and samples with different nucleating agent contents after isothermal crystallization. It can be observed that in the WAXD pattern of pure PPR without nucleating agent, 2θ = 14.2°, 17.1°, 18.9°, 21.5° and 22.2° typically correspond to the crystal plane (110), (040), (130), (111) and (−131) of α-crystal reflections, respectively. At the same time, a small amount of γ-crystal is naturally formed during isothermal crystallization, and 20.3° typically corresponds to γ-crystal plane (117).[46] With incorporating WBN-28 into PPR, the new β-crystal diffraction peak (300) crystal plane of PPR is typically at 2θ = 16.3°, and the β-crystal (311) crystal plane coincides precisely with the α-crystal plane (111), so the diffraction peak of about 21.5° still exists. The peak height of α-crystal plane (110) and (040) gradually decreases with the continual increase of nucleating agent addition. Except for pure

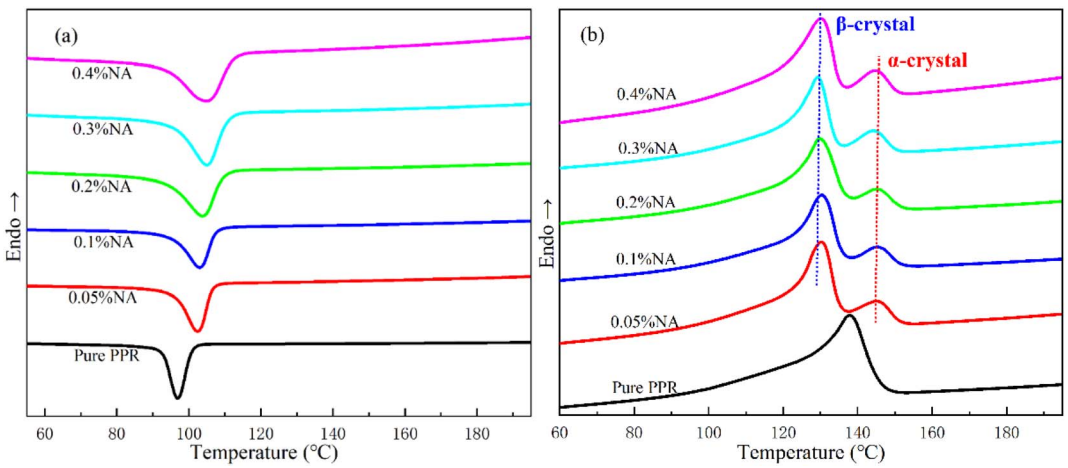

Fig. 1 (a) DSC cooling curves of pure PPR and PPR/NA blends; (b) DSC heating curves of pure PPR and PPR/NA blends.

Table 1 Crystallization and melting parameters of pure PPR and PPR/NA blends calculated from DSC curves

β-NA content%	T_c (°C)	$T_{m\beta}$ (°C)	$T_{m\alpha}$ (°C)	ΔH_α (J g^{-1})	ΔH_β (J g^{-1})	X_α (%)	X_β (%)	X (%)	φ_β (%)
0	96.8		137.8	52.3		29.5		29.5	0.0
0.05	102.5	130.2	145.0	7.2	43.5	4.1	25.8	29.9	86.4
0.1	103.0	130.5	145.2	6.4	44.2	3.6	26.2	29.8	87.9
0.2	103.9	129.9	145.1	6.1	45.5	3.5	27.0	30.4	88.7
0.3	105.1	129.3	144.2	6.8	52.3	3.9	31.0	34.9	88.9
0.4	105.1	130.2	144.6	6.6	53.5	3.7	31.8	35.5	89.5

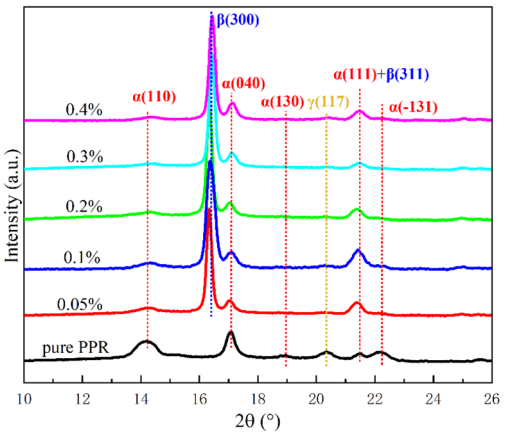

Fig. 2 WAXD patterns of pure PPR and PPR/NA blends.

PPR, all PPR/NA blends essentially have no diffraction peaks of α-crystal plane (130), (−131) and γ-crystal plane (117), indicating that the β-crystal induction effect of WBN-28 is extremely efficient, and an efficient β-crystal induction effect can be easily achieved at low concentration.

Fig. 3 shows the relative content of β-crystal calculated from DSC curves (φ_β) and WAXD data (K_β), respectively. The results show that the values of φ_β and K_β both surpass 85% in PPR/0.05NA. The values further increase slowly with the increment of nucleating agent. It can equally be exposed that the two fusion peaks are basically separated, and the eutectic regions of α- and β-crystals are very few from Fig. 1(b). In the system with the same addition amount, φ_β is consistently higher than K_β, but the observed difference between them is vastly small. It shows that the addition of nucleating agent into PPR induces single stable β-crystals. And it typically has a considered excellent β-crystal induction effect at a low concentration of 0.05%, which is more efficient than other reported nucleating agents in propylene–ethylene random copolymer.[47,48]

3.2 Isothermal crystallization analysis of PPR/NA

As shown clearly in Fig. 4, the β fusion peaks of each nucleating agent concentration are extremely significant during the secondary melting after isothermal crystallization at 116 °C. Except that the fusion peak of β-crystal with 0.2% addition (blue curve) shifts to elevated temperature, the peak positions of other concentrations are relatively immovable. A weak independent α-crystal fusion peak can still be observed in secondary melting curve after isothermal crystallization in PPR/0.05NA. There is only a little "subtle bulge" trend at the fusion peak of α-crystal, and the melting curve has become basically smooth in PPR/0.1NA. The fusion peaks of α- and β-crystal are completely fused into one peak, which leads to β fusion peak shift to the right elevated temperature in PPR/0.2NA. When the addition amount is more than 0.2%, the curve has only one independent β-crystal fusion peak, and it gradually returns to the lower temperature. The preceding phenomena indicate that when the addition of nucleating agent in PPR surpasses 0.2%, the crystal induced is essentially β form after isothermal crystallization at

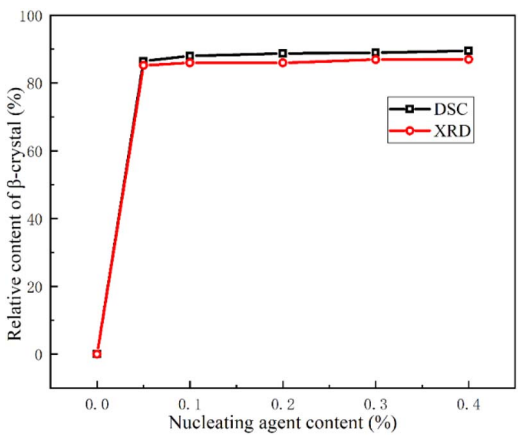

Fig. 3 Relative content of β-crystal calculated from the DSC and WAXD measurements.

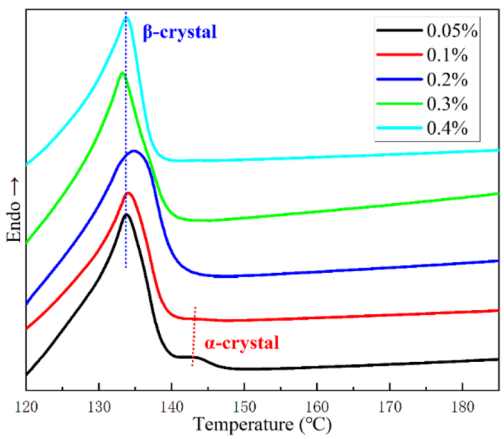

Fig. 4 DSC melting curves of PPR with different β-NA content after isothermal crystallization at 116 °C.

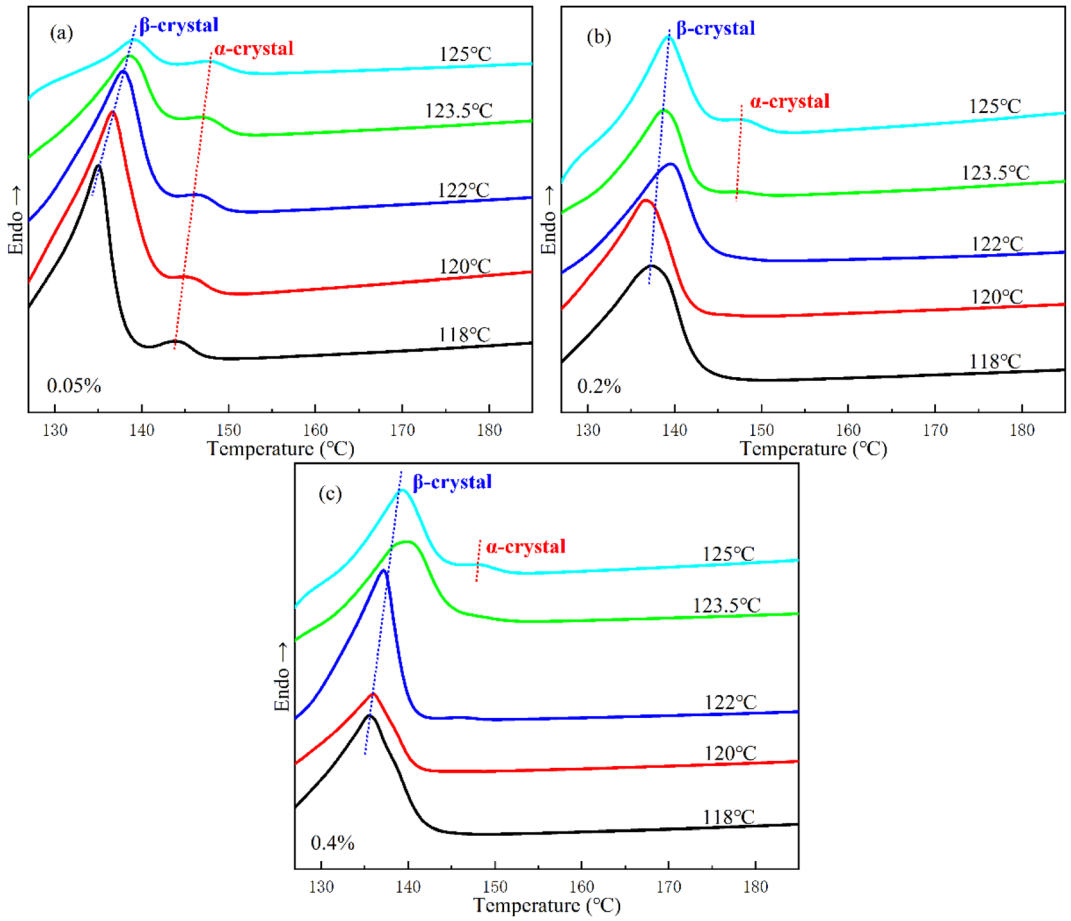

Fig. 5 DSC melting curves of PPR with 0.05% NA (a), 0.2% (b), 0.4% (c) after isothermal crystallization at different temperature for 1 hour.

116 °C. The high content of β-crystal inhibits the growth of α-crystal.

To further understand its nucleation characteristics, the isothermal crystallization curves with different nucleating agent contents after changed temperatures are recorded as shown in Fig. 5. The fusion peak temperatures of α- and β-crystal increase with increasing isothermal crystallization temperature due to the constant growth in the thickness of the lamellae. With the gradual increase of isothermal crystallization temperature, the fusion peak area of α-crystal does not change significantly in PPR/0.05NA (Fig. 5(a)). This indicates there is a small stationary amount of α-crystal. It also can be observed from Fig. 5(a) that when the isothermal crystallization temperature increases from 118 to 125 °C, the content of β-PP dropped a lot. It is because the growth rate of β-crystal slows down with the increase of isothermal crystallization temperature and the number of β-nuclei is insufficient. This no longer occurs in Fig. 5(b) and (c) with sufficient nucleating agent addition. Moreover, no obvious α-crystal fusion peak is observed in PPR/0.2NA (melting after 118–122 °C) and PPR/0.4NA (melting after 118–123.5 °C). This is because there are many nucleation sites of β-crystal, and the rapid expansion of β-crystal limits the growth of α-crystal at appropriate crystallization temperature. The βα-recrystallization[49] of PPR/0.2NA and PPR/0.4NA occurs at 122–123.5 °C and 123.5–125 °C, respectively. This is intimately related to the gradual decrease numbers of nucleation sites of α-crystal. The incredible high β-CR of WBN-28 successfully inhibits the growth of α-crystal and delays the βα-recrystallization.

3.3 Observation of crystal morphology

The growth process of polymer spherulites and the change of crystal morphology can be observed intuitively by polarizing microscope. In addition, α-crystal and β-crystal can be clearly distinguished according to the polarizing system.[50] Fig. 6 shows the polarized crystalline morphology of pure PPR and PPR with different nucleating agent concentrations after isothermal crystallization at 120 °C. It can be observed from Fig. 6(a) that the pure PPR typically has a large spherulite size. Because the PPR molecular chain naturally contains some ethylene segments, the spherulite morphology is not as complete and clear as that in PPH. Despite this, the obvious cross-polarization effect can still be observed. A massive number of crystal nuclei are produced, the crystal grains are obviously refined with adding the nucleating agent. The polarization effect of all the blends with nucleating agents is not as noticeable as that of pure PPR in Fig. 6(b)–(f). Except for a small amount of α polarization effect in PPR/0.05NA, no obvious α cross polarization phenomenon is found in the other blends. It shows that there is

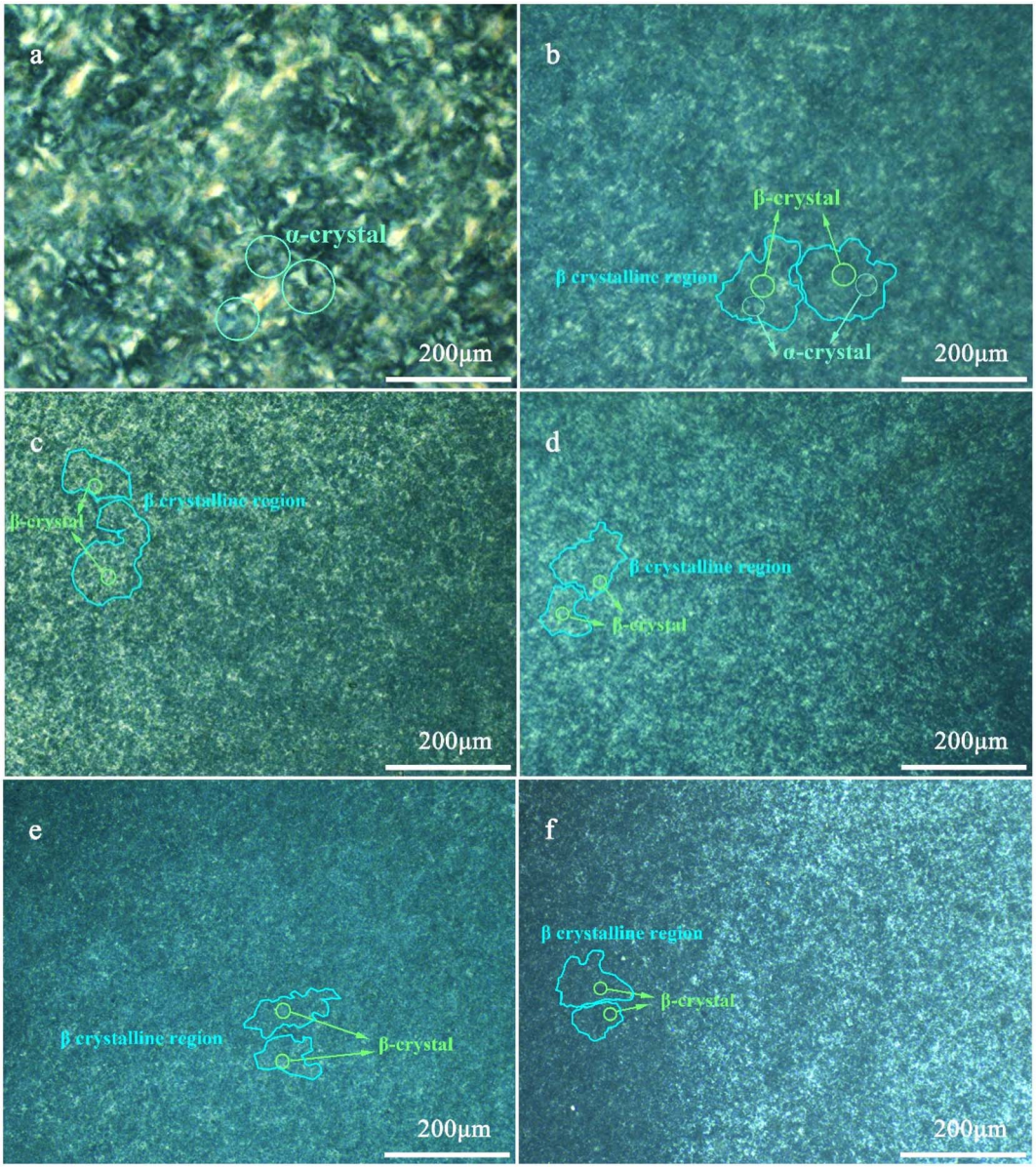

Fig. 6 POM photographs of pure PPR (a) and PPR with 0.05% NA (b), 0.1% NA (c), 0.2% NA (d), 0.3% NA (e), 0.4% NA (f) isothermal crystallization at 120 °C.

not enough α lamellae to form when the blends are isothermally crystallized at 120 °C. This is consistent with the result that only the β fusion peak is observed in the secondary melting curve after isothermal crystallization. In addition, it can be clearly observed that after isothermal crystallization, some irregular plate-like crystalline regions are naturally formed in the blends. With the increase of the nucleating agent amount, the crystal density in the blends is clearly improved. During the growth of β-crystal, it is easy to encounter other spherulites, so the size of spherulites is decreasing and rapidly connected into a crystalline region.

In the gradual process of β-crystal formation, the PP molecular chain segments are first arranged on the surface of the ordered structure of the nucleating agent to start crystallization. Further, the PP molecular chains are folded and properly arranged into the β-crystal lattice and formed β-crystal.[51] Although the specific composition of the β-NA is not clear, it can be observed from Fig. 7(a) that WBN-28 possesses a certain regular stacked crystal structure. Additionally, WBN-28 undoubtedly possesses a significant crystal structure from WAXD patterns in Fig. 7(b). The relative intensity of the other peaks is extremely low. It sufficiently indicates there is a highly ordered structure in WNB-28, the periodicity of 12.89 Å, which corresponds to the diffraction peak of crystalline at 6.85°. The highly ordered structure of WBN-28 can act as growth surface, which in turn induces PP molecular chain epitaxial to crystallize on it.

According to theory of epitaxial crystallization, the periodicity of substrates can match the chain periodicity in the *c*

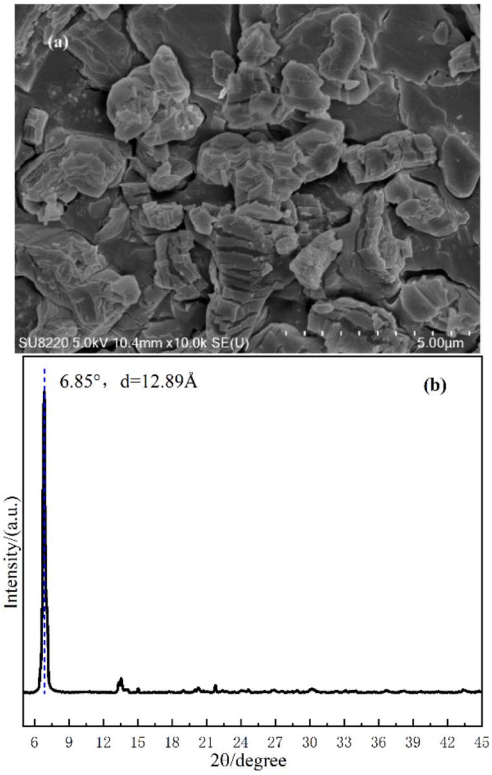

Fig. 7 (a) SEM of β nucleating agent WBN-28; (b) WAXD patterns of WBN-28.

direction of β-PP, and the mismatch ratio (M_r) should be less than 15%.[52,53] The mismatch ratio between c direction of β-PP and ordered structure of WBN-28 can be calculated in the following equation:

$$M_r = \frac{2 \times c_{\beta PP} - d}{d} \times 100\% \quad (8)$$

The calculation result of M_r is 0.85%, which is the lowest mismatch rate reported in the literatures.[54,55] As shown in Fig. 8, the ordered structure of the nucleating agent WBN-28 is highly matched with the periodicity of the c-axis of polypropylene. Based on this, the ordered structure of WBN-28 can be used as

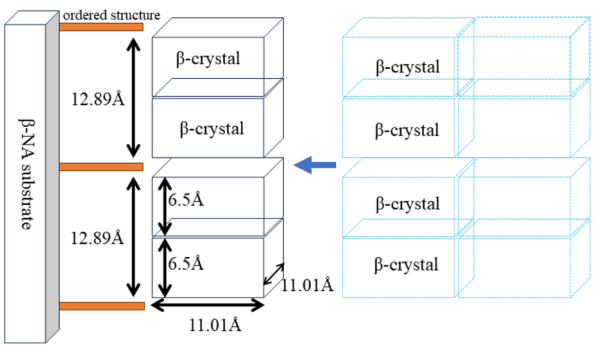

Fig. 8 Proposed nucleation mechanism of WBN-28 during the crystallization of PPR. The lattice constants of β-PP were quoted from the literature.[56]

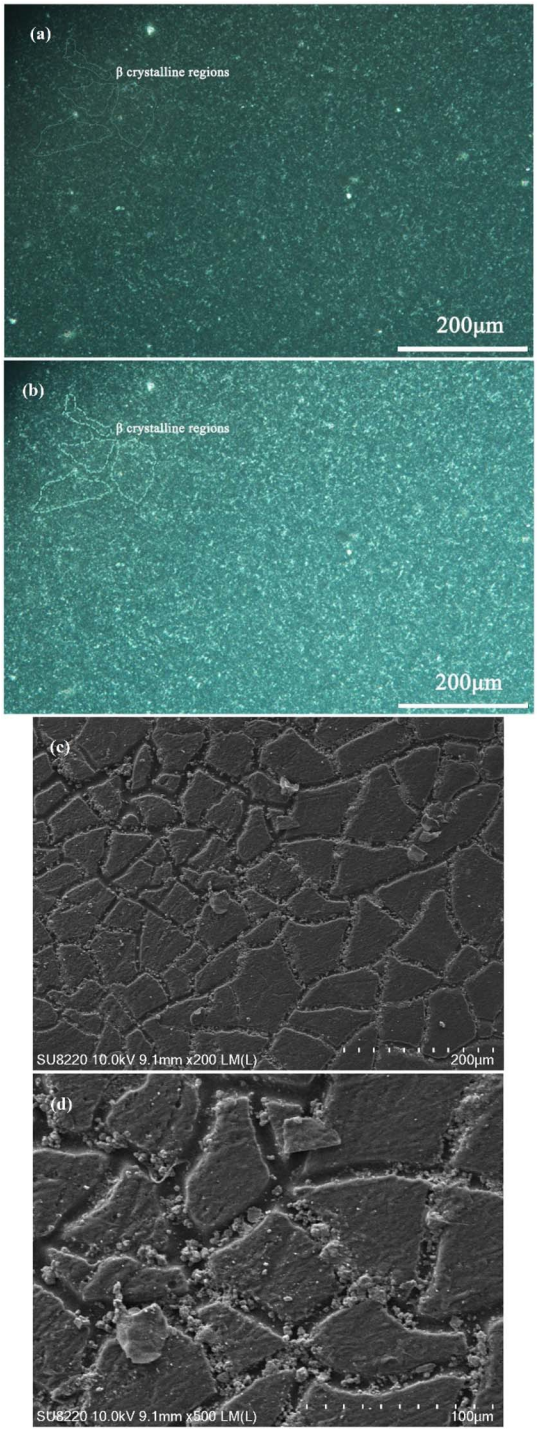

Fig. 9 POM photographs of PPR/0.2NA during isothermal crystallization at 120 °C for 30S (a) and 120S (b) (four β crystalline regions have been marked); SEM photographs of PPR/0.2NA after isothermal crystallization at 120 °C ×200 (c) and ×500 (d).

an epitaxial nucleation center to adsorb PP chains and significantly accelerate the nucleation process. Further, the β lattice continues to stack to thicken the crystalline region. Therefore, it can be observed that the crystallization area gradually becomes brighter but the size is remarkably unchanged by utilizing the polarizing microscope from Fig. 9(a) and (b).

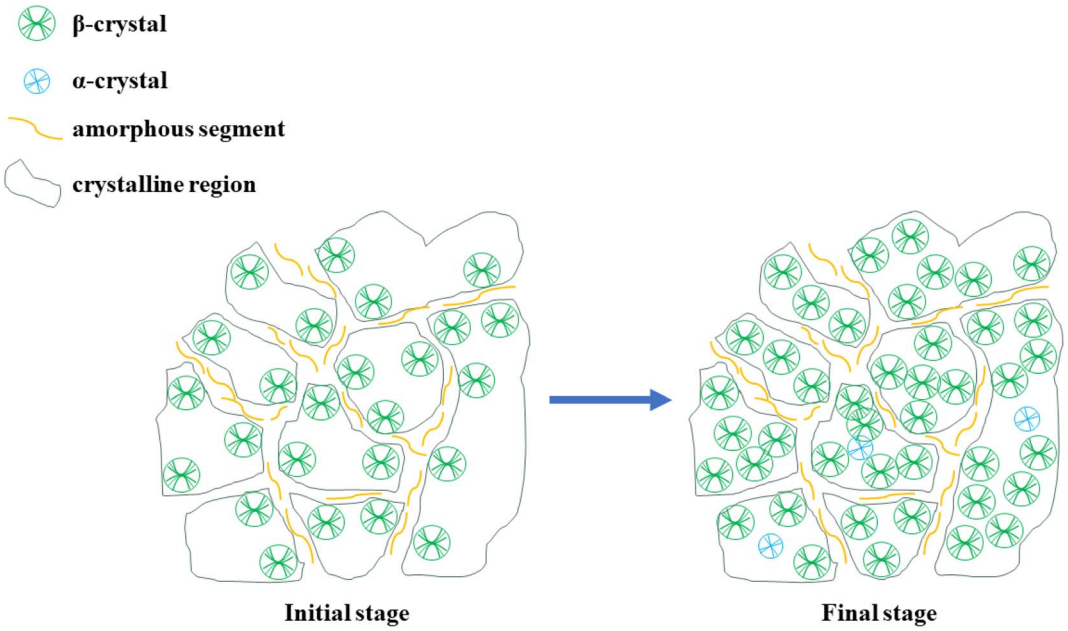

Fig. 10 Proposed schematic diagram of naturally forming process of β crystalline regions.

At the initial stage of isothermal crystallization at 120 °C, a substantial number of irregular crystalline regions are naturally formed in PPR/0.2NA, as shown in Fig. 9(a). To make it easier to correctly distinguish, four β crystalline regions are precisely identified. With the gradual increase of isothermal crystallization time, the specific size of β crystalline region does not change significantly. The brighter picture Fig. 9(b) shows that enough crystals are being created in continuous succession. The scanning electron microscope of the etched sample can visually observe the morphological characteristics of the crystalline region. The crystalline regions appear as irregular plate-like distribution, and there is obvious etching gully between the plates, which precisely represent the etched amorphous area related to the ethylene segments. Some of the particles in the etched grooves are incompletely washed potassium permanganate particles. Further magnifying the Fig. 9(c), there are some regular distribution "lines" on the plate-like crystalline region, which is reasonably the β-crystal supramolecular structure of PPR.[57]

The forming process of β crystalline regions are proposed in Fig. 10. Combined with the previous isothermal crystallization analysis, after β-NA is added into PPR, there are only a small number of fixed α-crystal nuclei in PPR. When the addition amount is more than 0.2%, the fusion peak of α-crystal is scarcely observed in the secondary melting curve after isothermal crystallization. It sufficiently indicates that β-crystal induction is absolutely dominant in PPR isothermal crystallization. With the passage of time, the thickness of the crystalline region increases. Simultaneously, the polarization effect is more significant, while the size of the crystalline region does not change significantly. In addition, the size of the crystalline region is equally related to the inherent defects of the molecular chain. Because of the presence of ethylene copolymerization unit, it is impossible to naturally produce a completely uniform crystal size in the PPR/NA blends.

In the early stage of crystallization, due to the high lattice matching between WBN-28 and β-PP, β-crystal will be rapidly produced. At the same time, suiting to the distribution of the surrounding molecular chains, different sizes of fixed β-crystal regions are instantly formed. For another thing, there is naturally a certain amorphous region in the matrix, and the molecular chain of the amorphous region is squeezed by the crystalline region. It can exclusively be distributed in the matrix in a narrow arrangement. This shows that the amorphous region and the crystal region have achieved precisely a clear "segmentation" in a relatively transitory period of time, dividing their respective "spheres of influence". As the crystallization time increases, more molecular chains fold into the β lattice.[57] The continuous stacking of β lattices and the formation of a small number of α-crystals in the β-crystal region increases the polarization effect of the crystal region.

4 Conclusion

In summary, a new efficient rare earth β-NA for PPR was firstly reported in this paper, which could be directly added to procure high β-CR. The β-CR calculated by DSC and WAXD could both surpass 85% when the nucleating agent content was mere 0.05%. With the increment of nucleating agent, the β-CR increased further. The conversion rate calculated by DSC and WAXD was not significantly different, which proved that WBN-28 naturally has a notable single β-crystal induction effect, which is undoubtedly the most efficient β-NA directly added into PPR as known at present. When the addition amount was more than 0.2%, the fusion peak of α-crystal was unobserved on the secondary melting curve after isothermal crystallization at

116 °C. With the gradual increase of isothermal crystallization temperature, the fusion peak area of α-crystal did not change significantly in PPR/0.05NA. In addition, only a small amount of α-crystal melting peaks can be justly observed at 123.5 °C and 125 °C in PPR/0.2NA and PPR/0.4NA, respectively. Meanwhile, βα-recrystallization also occurred at the corresponding more elevated temperature. The addition of β-NA significantly increased the crystallization rate, which made the β-crystal grain in PPR more refined. A small amount of α-crystal cross-polarization effect can be justly observed only in PPR/0.05NA. During the growth of β-crystal, the rapidly growing spherulites were easy to encounter the others. The spherulites were continuously stacked, and the amorphous regions in the blends were squeezed, so rapidly connected into a plate-like crystalline region. The high lattice matching between the ordered structure of WBN-28 with the periodicity of 12.89 Å and the *c*-axis of β-PP was the main reason for the previous results. This work is beneficial to further understand the effect of β-NA on PPR β-modification and undoubtedly provide a more appropriate choice for its engineering application.

Author contributions

Bo Wu: conceptualization, writing – original draft, formal analysis. Xian Zheng: formal analysis, writing – review & editing. Yanwei Ren: investigation. Hailong Yu: softwore. Haiqiang Leng: resources. Yubo Wang: data curation. Huanfeng Jiang: conceptualization, validation, funding acquisition.

Conflicts of interest

There are no conflicts to declare.

Acknowledgements

The authors thank the National Key Research and Development Program of China (2022YFB4101800), the National Natural Science Foundation of China (22231002), and the Cooperate Research Project for Guangdong Winner New Materials Technology Co., Ltd. for financial support.

References

1 Y. Feng and J. N. Hay, *Polymer*, 1998, **39**, 6723–6731.
2 M. Seki, H. Nakano, S. Yamauchi, J. Suzuki and Y. Matsushita, *Macromolecules*, 1999, **32**, 3227–3234.
3 Z. Q. Wang, Y. F. Zhang, Y. Li and J. R. Zhong, *Polym. Bull.*, 2023, **80**, 3103–3117.
4 X. Guo, Y. Chen, J. Guo, J. Qin, H. Lian, Z. Lu and X. Chen, *Polym. Eng. Sci.*, 2023, **63**, 1989.
5 L. Yu, T. Wu, T. Chen, F. Yang and M. Xiang, *Thermochim. Acta*, 2014, **578**, 43–52.
6 J. Zheng, J. Zhang, J. Xu, C. Liu and L. Xu, *Eng. Failure Anal.*, 2020, **117**, 104831.
7 D. G. Papageorgiou, D. N. Bikiaris and K. Chrissafis, *Thermochim. Acta*, 2012, **543**, 288–294.
8 J. Cao, Y. Zheng and T. Lin, *Polym. Test.*, 2016, **55**, 318–327.
9 D. G. Papageorgiou, G. Z. Papageorgiou, D. N. Bikiaris and K. Chrissafis, *Eur. Polym. J.*, 2013, **49**, 1577–1590.
10 B. Wu, X. Zheng, W. Xu, Y. Ren, H. Leng, L. Liang, D. Zheng, J. Chen and H. Jiang, *Polymers*, 2023, **15**, 3107.
11 S. Mishra, S. H. Sonawaen and R. P. Singh, *J. Polym. Sci., Part B: Polym. Phys.*, 2005, **43**, 107–113.
12 J. Liu and H. Liang, *J. Therm. Anal. Calorim.*, 2021, **146**, 2115–2126.
13 L. Liu, Y. Zhao, C. Zhang, Z. Dong, K. Wang and D. Wang, *Macromolecules*, 2021, **54**, 6824–6834.
14 F. Horváth, D. Bodrogi, B. Hilt, E. Pregi and A. Menyhárd, *J. Therm. Anal. Calorim.*, 2022, **147**, 9451–9468.
15 F. Horváth, L. Bihari, D. Bodrogi, T. Gombár, B. Hilt, B. Keszei, T. Krain, A. Simon and A. Menyhárd, *ACS Omega*, 2021, **6**, 9053–9065.
16 Y. M. Liu, Z. Z. Tong, J. T. Xu, Z. S. Fu and Z. Q. Fan, *J. Appl. Polym. Sci.*, 2014, **131**, 40753.
17 S. Zhao, N. Xu, Z. Xin and C. Jiang, *J. Appl. Polym. Sci.*, 2012, **123**, 108–117.
18 T. Song, Z. Ren, H. Li, X. Sun, M. Xue and S. Yan, *Composites, Part A*, 2019, **123**, 200–207.
19 J. Feng, M. Chen, Z. Huang, Y. Guo and H. Hu, *J. Appl. Polym. Sci.*, 2002, **85**, 1742–1748.
20 C. Ding, G. G. Wu, Y. Zhang, W. B. Chen, B. Yin and M. B. Yang, *Polym. Cryst.*, 2019, **2**, e10080.
21 S. Nie, J. R. Zhong, Y. Li and Y. F. Zhang, *J. Therm. Anal. Calorim.*, 2023, **148**, 6097–6106.
22 J. Liu, X. Zhu and Z. Cao, *Polymers*, 2019, **11**, 1894.
23 J. Liu and T. Zhu, *Polym. Bull.*, 2021, **78**, 3259–3274.
24 Y. Li, M. Li, M. Nie, Q. Wang and R. Han, *J. Mater. Sci.*, 2017, **52**, 981–992.
25 H. Bai, F. Luo, T. Zhou, H. Deng, K. Wang and Q. Fu, *Polymer*, 2011, **52**, 2351–2360.
26 W. Qin, Z. Xin, C. Pan, S. Sun, X. Jiang and S. Zhao, *Chem. Eng. J.*, 2019, **358**, 1243–1252.
27 J. Zhu, H. Ni, X. Liao and X. Liu, *J. Chem.*, 2015, **2015**, 545016.
28 X. Zhang and G. Shi, *Thermochim. Acta*, 1994, **235**, 49–59.
29 J. Cao and Q. F. Lü, *Polym. Test.*, 2011, **30**, 899–906.
30 J. Fan and J. Feng, *Ind. Eng. Chem. Res.*, 2013, **52**, 761–770.
31 K. Busse and J. Kressler, *Macromolecules*, 2000, **33**, 8775–8780.
32 J. Fu, X. Li, M. Zhou, R. Hong and J. Zhang, *Polym. Bull.*, 2019, **76**, 865–881.
33 H. Zheng, F. Zeng, Z. Chen, J. Kang, J. Chen, Y. Cao and M. Xiang, *J. Polym. Res.*, 2017, **24**, 225.
34 B. Na, R. Lv, W. Xu, R. Chen, Z. Zhao and Y. Yi, *Polym. Int.*, 2008, **57**, 1128–1133.
35 D. G. Papageorgiou, G. Vourlias, D. N. Bikiaris and K. Chrissafis, *Macromol. Mater. Eng.*, 2014, **299**, 707–721.
36 J. Lin, H. Wei, J. Su, X. Li, J. Huang, S. Anwer, S. Liang, G. Cong, L. Xu, F. Lu and M. Ji, *Front. Chem.*, 2022, **10**, 01–02.
37 M. Li, G. Li, Z. Zhang, X. Dai and K. Mai, *Thermochim. Acta*, 2014, **598**, 36–44.
38 A. Menyhárd, J. Varga, Á. Liber and G. Belina, *Eur. Polym. J.*, 2005, **41**, 669–677.
39 F. Luo, Y. Zhu, K. Wang, H. Deng, F. Chen, Q. Zhang and Q. Fu, *Polymer*, 2012, **53**, 4861–4870.

40 Y. Li, M. Nie and Q. Wang, *Polym. Eng. Sci.*, 2016, **56**, 866–873.
41 N. Jiang, K. Wang, J. Leng and B. He, *Polym. Bull.*, 2018, **75**, 4085–4101.
42 J. X. Li, W. L. Cheung and D. Jia, *Polymer*, 1999, **40**, 1219–1222.
43 M. Liu, B. Guo, M. Du, F. Chen and D. Jia, *Polymer*, 2009, **50**, 3022–3030.
44 A. Turner Jones, J. M. Aizlewood and D. R. Beckett, *Macromol. Chem. Phys.*, 1964, **75**, 134–158.
45 X. Wang, J. Dai, J. Chen, J. Duan, J. Yang, J. Zhang and Y. Wang, *Ind. Eng. Chem. Res.*, 2015, **54**, 4976–4987.
46 J. Wang, M. Gahleitner, D. Gloger and K. Bernreitner, *eXPRESS Polym. Lett.*, 2020, **14**, 491–502.
47 X. Zhang, F. Tang, W. Lv, H. Wu, X. He and S. Zhao, *J. Polym. Res.*, 2022, **29**, 4.
48 F. Horváth, D. Bodrogi, B. Hilt, E. Pregi and A. Menyhárd, *J. Therm. Anal. Calorim.*, 2022, **147**, 9451–9468.
49 Q. Yuan, W. Jiang and L. An, *Colloid Polym. Sci.*, 2004, **282**, 1236–1241.
50 B. Lotz, *Polymer*, 1998, **39**, 4561–4567.
51 R. Yang, L. Ding, W. Chen, L. Chen, X. Zhang and J. Li, *Macromolecules*, 2017, **50**, 1610–1617.
52 Y. Yue, D. Hu, Q. Zhang, J. Lin and J. Feng, *Polymer*, 2018, **149**, 55–64.
53 J. Wittmann, A. Hodge and B. Lotz, *J. Polym. Sci., Part B: Polym. Phys.*, 1983, **21**, 2495–2509.
54 S. Liu, J. Yang, Q. Liu, Y. Huang, M. Kong, Q. Yang and G. Li, *Chem. Eng. J.*, 2019, **363**, 1–12.
55 Y. Sun, S. Zhao, X. Zhang, C. Tong, W. Qin and Z. Xin, *Ind. Eng. Chem. Res.*, 2020, **59**, 18529–18538.
56 S. V. Meille, D. R. Ferro, S. Brueckner, A. J. Lovinger and F. J. Padden, *Macromolecules*, 1994, **27**, 2615–2622.
57 C. Mathieu, A. Thierry, J. C. Wittmann and B. Lotz, *J. Polym. Sci., Part B: Polym. Phys.*, 2002, **40**, 2504–2515.